



**HAL**  
open science

## Magnetic fabric of sheared till: A strain indicator for evaluating the bed deformation model of glacier flow

Thomas S. Hooyer, Neal R. Iverson, France Lagroix, Jason F. Thomason

### ► To cite this version:

Thomas S. Hooyer, Neal R. Iverson, France Lagroix, Jason F. Thomason. Magnetic fabric of sheared till: A strain indicator for evaluating the bed deformation model of glacier flow. *Journal of Geophysical Research: Earth Surface*, 2008, 113, 10.1029/2007JF000757 . insu-01311127

**HAL Id: insu-01311127**

**<https://insu.hal.science/insu-01311127>**

Submitted on 3 May 2016

**HAL** is a multi-disciplinary open access archive for the deposit and dissemination of scientific research documents, whether they are published or not. The documents may come from teaching and research institutions in France or abroad, or from public or private research centers.

L'archive ouverte pluridisciplinaire **HAL**, est destinée au dépôt et à la diffusion de documents scientifiques de niveau recherche, publiés ou non, émanant des établissements d'enseignement et de recherche français ou étrangers, des laboratoires publics ou privés.

## Magnetic fabric of sheared till: A strain indicator for evaluating the bed deformation model of glacier flow

Thomas S. Hooyer,<sup>1</sup> Neal R. Iverson,<sup>2</sup> France Lacroix,<sup>3</sup> and Jason F. Thomason<sup>2,4</sup>

Received 17 January 2007; revised 21 August 2007; accepted 14 December 2007; published 5 April 2008.

[1] Wet-based portions of ice sheets may move primarily by shearing their till beds, resulting in high sediment fluxes and the development of subglacial landforms. This model of glacier movement, which requires high bed shear strains, can be tested using till microstructural characteristics that evolve during till deformation. Here we examine the development of magnetic fabric using a ring shear device to deform two Wisconsin-age basal tills to shear strains as high as 70. Hysteresis experiments and the dependence of magnetic susceptibility of these tills on temperature demonstrate that anisotropy of magnetic susceptibility (AMS) develops during shear due to the rotation of primarily magnetite particles that are silt sized or smaller. At moderate shear strains ( $\sim 6$ – $25$ ), principal axes of maximum magnetic susceptibility develop a strong fabric ( $S_1$  eigenvalues of 0.83–0.96), without further strengthening at higher strains. During deformation, directions of maximum susceptibility cluster strongly in the direction of shear and plunge “up-glacier,” consistent with the behavior of pebbles and sand particles studied in earlier experiments. In contrast, the magnitude of AMS does not vary systematically with strain and is small relative to its variability among samples; this is because most magnetite grains are contained as inclusions in larger particles and hence do not align during shear. Although processes other than pervasive bed deformation may result in strong flow parallel fabrics, AMS fabrics provide a rapid and objective means of identifying basal tills that have not been sheared sufficiently to be compatible with the bed deformation model.

**Citation:** Hooyer, T. S., N. R. Iverson, F. Lacroix, and J. F. Thomason (2008), Magnetic fabric of sheared till: A strain indicator for evaluating the bed deformation model of glacier flow, *J. Geophys. Res.*, 113, F02002, doi:10.1029/2007JF000757.

### 1. Introduction

[2] Shear deformation of weak sediment beneath ice sheets may be a common mechanism of glacier flow [Clarke, 2005]. If pervasive over a sufficiently large thickness of the bed, this deformation may also result in large fluxes of sediment to the margins of glaciers [e.g., Alley, 1991, 2000; Jenson *et al.*, 1995; Hooke and Elverhøi, 1996; Dowdeswell and Siegert, 1999] and the development of diverse landforms [e.g., Hindmarsh, 1988; Johnson and Hansel, 1999; Fowler, 2000; Ó Cofaigh *et al.*, 2005]. A fundamental requirement of the bed deformation model is that glacier movement occurs primarily by shear deformation of the bed, such that basal sediment is sheared to very high strains. Even for short periods of glacier occupation (e.g., 100 years) and low glacier speeds, basal displace-

ments by bed deformation should exceed 1000 m, indicating shear strains of  $\sim 10^2$  to  $10^4$  for reasonable thicknesses of shearing bed sediment (0.1–10 m).

[3] The most common subglacial sediment is probably till. Many observations of structures at various scales in basal tills demonstrate that they have been deformed [e.g., Menzies, 2000; van der Wateren *et al.*, 2000; van der Meer *et al.*, 2003]. These observations are not surprising because, regardless of how till accumulates subglacially, some deformation is expected. For example, when a glacier slides over till, particles that partially protrude from the glacier sole will plow through underlying sediments and can ultimately lodge in the substrate. This lodgment process will locally deform the bed near plowing particles [e.g., Clark and Hansel, 1989; Jørgensen and Piotrowski, 2003]. Some deformation will also occur by consolidation when debris melts out of basal ice.

[4] Thus, in attempting to use the geologic record to test the bed deformation hypothesis, the key question is not whether till has been deformed but how much. This is a particularly hard question to answer for macroscopically homogeneous basal tills, with no obvious primary structures to use as strain indicators.

[5] The orientations of particles of many sizes in tills have been used to infer their depositional processes and strain histories. Unfortunately, interpretations of fabric usually

<sup>1</sup>Wisconsin Geological and Natural History Survey, University of Wisconsin, Madison, Wisconsin, USA.

<sup>2</sup>Department of Geological and Atmospheric Sciences, Iowa State University, Ames, Iowa, USA.

<sup>3</sup>Equipe de Paléomagnétisme, Institut de Physique du Globe de Paris, Université Paris Diderot, CNRS, Paris, France.

<sup>4</sup>Now at Illinois State Geological Survey, Champaign, Illinois, USA.

have been made with limited knowledge of formative physical processes and without the benefit of experimental data. Such is the case for basal tills inferred to have been sheared to high strains. For example, the interpretation of some field studies is that shear deformation can result either in a weak fabric parallel to the direction of glacier flow or in transverse fabrics [e.g., *Hicock and Dreimanis*, 1992; *Hart*, 1994; *Carr and Rose*, 2003]. Strong flow-parallel fabrics have sometimes been interpreted to be the result of lodgment [e.g., *Dowdeswell and Sharp*, 1986; *Hart*, 1994, 1997]. In contrast, laboratory studies of pebble and sand fabric in sheared till show that strong fabrics develop in the direction of shearing at relatively low shear strains (<10) and remain strong and parallel to the shearing direction at higher strains [*Hooyer and Iverson*, 2000a; *Thomason and Iverson*, 2006]. These results agree with the conclusions of *Benn* [1995], who studied particle fabrics in till that had been sheared beneath Breidamerkurjokull, Iceland [*Boulton and Hindmarsh*, 1987] and with some other field interpretations [*Benn and Evans*, 1996].

[6] There are clear drawbacks, however, to the use of pebble and sand fabrics for inferring strain. The relatively low density of pebbles in many tills limits the spatial resolution of pebble fabrics to zones in the bed that may be thicker than zones where shear deformation occurred. Sand particles are far more numerous in tills than pebbles but are usually studied optically, requiring tedious till impregnation with epoxy and the production of thin sections. Moreover, to obtain three-dimensional sand fabrics orthogonal thin sections must be made, with assumptions regarding statistical uniformity of grain orientations among these sections. In addition, measurement of both pebble and sand fabrics cannot be fully automated, such that human subjectivity adds measurement error. The magnitude of this human error is seldom quantified, thereby limiting the value of interpretations.

[7] An alternative to measuring orientations of particles directly is to measure the anisotropy of magnetic susceptibility (AMS) of multiple intact till specimens. A small specimen (usually 1–12 cm<sup>3</sup>) is subjected at many orientations to a uniform magnetic field to determine an AMS ellipsoid that represents the anisotropy of the magnetization induced by the specimen. In rocks and sediments orientations of AMS ellipsoids have been found to commonly correspond to the shape-preferred orientations of strongly magnetic particles, such as magnetite, maghemite, and pyrrhotite and to the crystallographic preferred orientation of more weakly magnetic, diamagnetic, or paramagnetic particles (see reviews by *Tarling and Hrouda* [1993] and *Borradaile and Jackson* [2004]). This technique has higher spatial resolution than pebble fabrics, does not require impregnation of till with epoxy or thin-section preparation, provides three-dimensional data, and involves less human subjectivity than measurements of individual particles. In addition, this technique averages over a volume that contains many more particles than can be measured individually.

[8] Although AMS of sediments, including tills, has been used to try to infer depositional processes [e.g., *Fuller*, 1964; *Gravenor et al.*, 1973; *Stupavsky et al.*, 1974a, 1974b; *Stupavsky and Gravenor*, 1975; *Easterbrook*, 1988; *Eyles et al.*, 1987; *Lagroix and Banerjee*, 2002, 2004], there have

been no attempts to correlate AMS data to strain magnitude in tills. In contrast, AMS is used commonly to infer the strain history of rocks [e.g., *Tarling and Hrouda*, 1993; *Borradaile and Jackson*, 2004] and fault gouge [*Hayman et al.*, 2004]. This work includes theoretical modeling of AMS development with strain [*Owens*, 1974; *Hrouda and Jeek*, 1999], as well as numerous laboratory experiments aimed at revealing the relationship between AMS and strain magnitude [e.g., *Borradaile and Alford*, 1987, 1988; *Arch et al.*, 1987; *Maltman*, 1987; *Borradaile and Puumala*, 1989; *Borradaile*, 1991].

[9] The objective of this study was to develop AMS-based proxies for shear strain in basal tills collected from two different lobes of the Laurentide Ice Sheet. We sheared remolded samples of these tills in experiments to various strains using a ring shear device, and the AMS of multiple samples was measured after each experiment. Both the shapes and alignment of AMS ellipsoids were compared with strain direction and magnitude. Results indicate that the fabric formed by the long axes of AMS ellipsoids lies parallel to the shearing direction and strengthens systematically with strain. Additional rock magnetic analyses indicate that this AMS fabric is caused by the alignment of primarily magnetite particles consisting of fine silt. These laboratory results provide a method for estimating strain magnitude in basal tills.

## 2. Methodology

### 2.1. Apparatus

[10] Our ring shear device shears a saturated till sample under a steady normal stress and shearing rate to whatever shear displacement is desired (Figure 1). The till is contained within an annular chamber that has an outside diameter of 0.6 m, a width of 0.115 m, and a maximum height of 0.08 m. The till is sandwiched by two permeable platens containing teeth that grip the sample. Water can leave or enter the till through these platens, which are connected to a reservoir at atmospheric pressure. The lower platen is anchored to a rotating base plate that is driven at a constant speed by a motor and gearboxes. The sample chamber is bound laterally by walls that are split in two roughly equal halves. The upper half is fixed whereas the lower wall is attached to the rotating base plate. As a result, shearing occurs in the middle of the specimen rather than adjacent to one of the platens, usually in a zone that is 10–35 mm in thickness at the specimen centerline [*Iverson et al.*, 1997; *Hooyer and Iverson*, 2000a, 2000b]. A downward stress normal to the plane of shearing is applied to the specimen with dead weights on a lever arm that presses on a thick plate (normal-load plate) that is connected to the upper platen. During shearing this normal-load plate can move vertically with dilation or consolidation of the till. This vertical motion is measured by three displacement transducers located around the perimeter of the normal-load plate. More detailed descriptions of the ring shear device are provided elsewhere [*Iverson et al.*, 1997, 1998; *Hooyer and Iverson*, 2000a].

### 2.2. Experimental Procedure

[11] A total of 13 experiments were performed with two different late Wisconsin-age basal tills deposited beneath

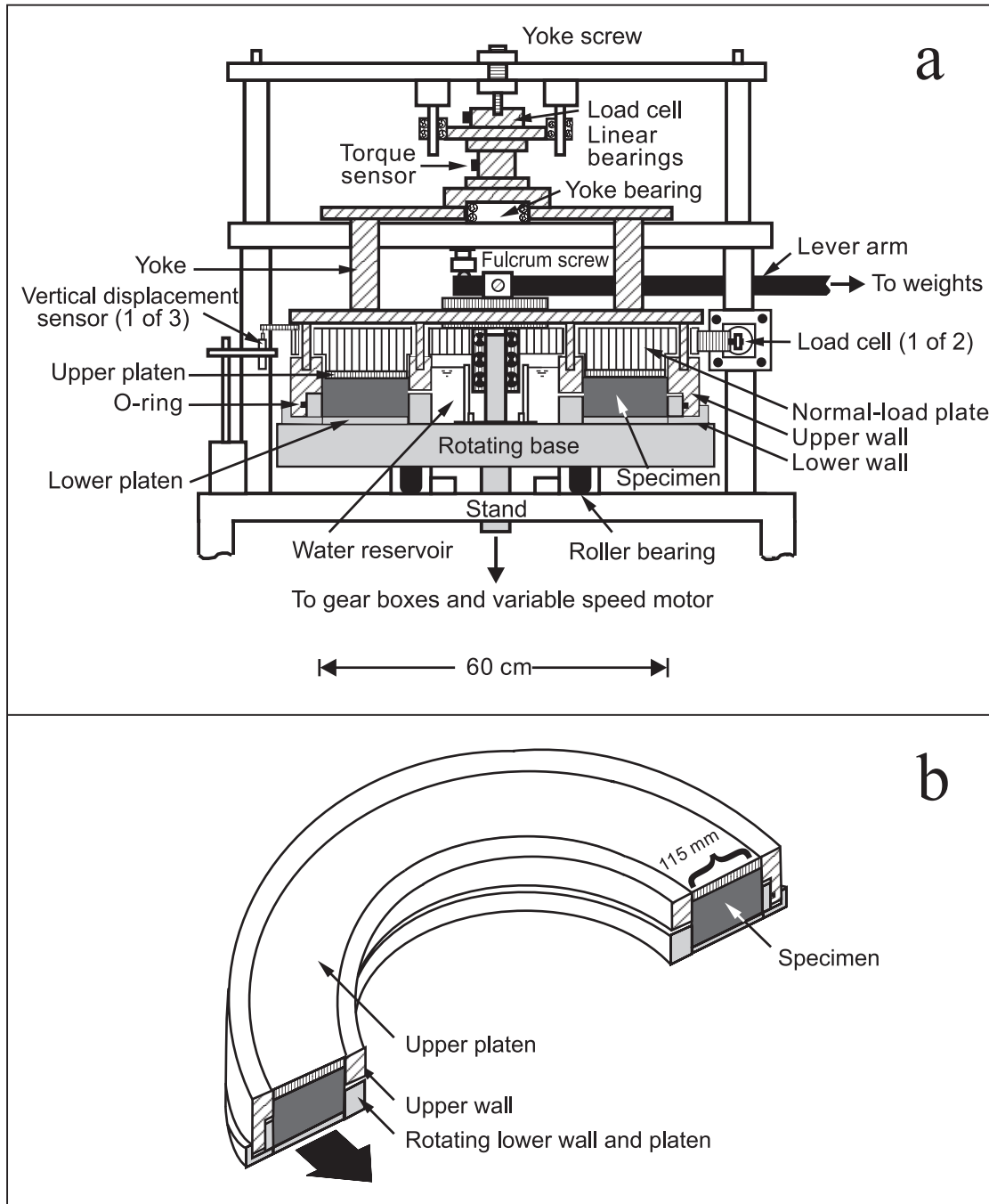


**Figure 1.** (a) Cross section of the ring shear device and (b) detail of the sample chamber. Solid light gray components rotate.

different lobes of the Laurentide Ice Sheet. Six experiments, D-1 through D-6, were performed with the Douglas Member of the Miller Formation [Johnson, 1983], which was chosen because of its low carbonate content that enabled optical characterization of microstructures [Thomason and Iverson, 2006]. This till, which has a rusty red color, was deposited by the Lake Superior Lobe in northern Wisconsin and consists of 5% gravel, 72% sand, and 23% silt and clay. This till is sandier than the second till studied, the Bates-

town Member of the Wedron Formation, deposited by the Lake Michigan Lobe [Johnson and Hansel, 1999]. Seven experiments (B-7 through B-13) were performed on this till, which consists of 17% gravel, 49% sand, and 34% silt and clay. This till was studied because its deformation is thought by some to have been important in the flow and sediment transport of the Lake Michigan Lobe [Jenson et al., 1995, 1996; Boulton, 1996], and the degree of its deformation has been estimated in an ancillary field study [Thomason,

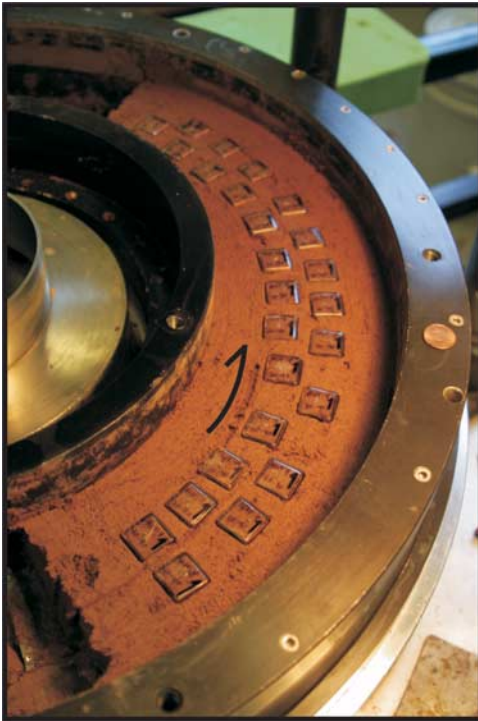


**Figure 2.** Plastic cubes pressed into the shear zone of the Douglas till after an experiment. The uppermost part of the till specimen has been removed to expose the shear zone. The width of the chamber of the ring shear device is 0.115 m. The solid black arrow indicates the direction of shearing (rotation direction of the rotating base).

2006]. In all experiments, particles  $>8$  mm in diameter were removed from both tills in accordance with geotechnical testing procedures [Head, 1989] that require removing grains larger than one-tenth of the minimum specimen dimension. By volume these particles were small fractions of the two tills: 3.4% of the Douglas till and 3.1% of the Batestown till.

[12] Prior to each experiment the till was fully saturated with distilled water and disaggregated. The initial water content prior to each experiment was 32% and 23% for the Douglas and Batestown tills, respectively. The till was then loaded into the sample chamber of the ring shear device. Before applying a normal stress to the till, it was remixed and three vertical columns of displacement markers, consisting of spherical wooden beads 4 mm in diameter, were placed across the width of the till to assess the postexperimental distribution of strain. The normal-load plate and upper platen were then positioned and weighted to apply a normal stress of 65 kPa, a value chosen to reflect the low effective normal stress beneath most sediment-floored glaciers [e.g., Engelhardt and Kamb, 1997]. Resultant consolidation of the till occurred for a period of hours as water was expelled from the pore space. Following consolidation either the ring shear device was disassembled and the till sampled, or the till was sheared at a steady rate of  $400 \text{ m a}^{-1}$ , where  $a$  is years, (about the speed of Whillans Ice Stream in West Antarctica [Engelhardt and Kamb, 1998]) to a predetermined displacement.

[13] Once shearing was complete, the normal stress on the till was removed, and the internal water reservoir was emptied. The displacement markers were then excavated to define the position and thickness of the zone of shearing within the specimen. Since this zone is centered at depth near the middle of the specimen, the upper unsheared layer of till was removed to expose the top of the shear zone. A minimum of 25 oriented small plastic boxes, cubes 18 mm on a side ( $5.8 \text{ cm}^3$ ) with a 1 mm wall thickness, were pressed into the sediment (Figure 2). Only the outermost 2 mm of till in the box were likely disturbed by this process [Tarling and Hrouda, 1993]. Samples were labeled to mark the shearing direction, carefully excavated, and sealed with a plastic cap.

[14] The AMS of the samples was studied using a Geofyzika KLY-2 KappaBridge AC Susceptibility Bridge. Each cube of till was subjected to a magnetic field of strength,  $H$ , in 15 different orientations [Jelinek, 1978]. The strength of the induced magnetization of the till  $M$  is given by  $kH$ , where the constant of proportionality  $k$  is called the susceptibility. In materials in which the shapes or crystallographic orientations of mineral grains have become aligned,  $k$  varies with direction, such that a second-rank tensor is required to characterize it [Tarling and Hrouda, 1993]. This tensor is best visualized with the susceptibility ellipsoid, which has lengths of its long, intermediate, and short axes equal to the principal susceptibilities  $k_1$ ,  $k_2$ , and  $k_3$ , respectively.

[15] To describe the shape of the AMS ellipsoid, which may vary with strain magnitude, we calculated various parameters commonly used to characterize the AMS of deformed rocks [Borradaile and Jackson, 2004]. A simple characterization of AMS-ellipsoid shape is the percent total anisotropy  $P\%$

$$P\% = 100 \left( \frac{k_1 - k_3}{k_v} \right), \quad (1)$$

where  $k_v$  is the volume susceptibility, defined as the mean of the principal susceptibilities [Tarling and Hrouda, 1993]. Two other useful parameters for describing the AMS ellipsoid include the shape parameter ( $T_j$ ) and the corrected degree of anisotropy ( $P_j$ ) [Jelinek, 1981]:

$$T_j = \frac{\ln\left(\frac{k_2}{k_3}\right) - \ln\left(\frac{k_1}{k_2}\right)}{\ln\left(\frac{k_2}{k_3}\right) + \ln\left(\frac{k_1}{k_2}\right)} \quad \text{and} \quad (2)$$

$$P_j = \exp \left( \sqrt{2 \left[ \left( \ln\left(\frac{k_1}{k}\right) \right)^2 + \left( \ln\left(\frac{k_2}{k}\right) \right)^2 + \left( \ln\left(\frac{k_3}{k}\right) \right)^2 \right]} \right). \quad (3)$$

If  $-1 \leq T_j < 0$ , the ellipsoid is prolate, and if  $0 < T_j \leq 1$ , the ellipsoid is oblate.  $P_j = 1$  if the ellipsoid is a sphere, and the value of  $P_j$  increases with increasing anisotropy. The advantages of these formulations for characterizing rock strain were discussed by Borradaile and Jackson [2004].

[16] In addition to assessing the shape of AMS ellipsoids, we studied their degree of alignment as a function of strain,

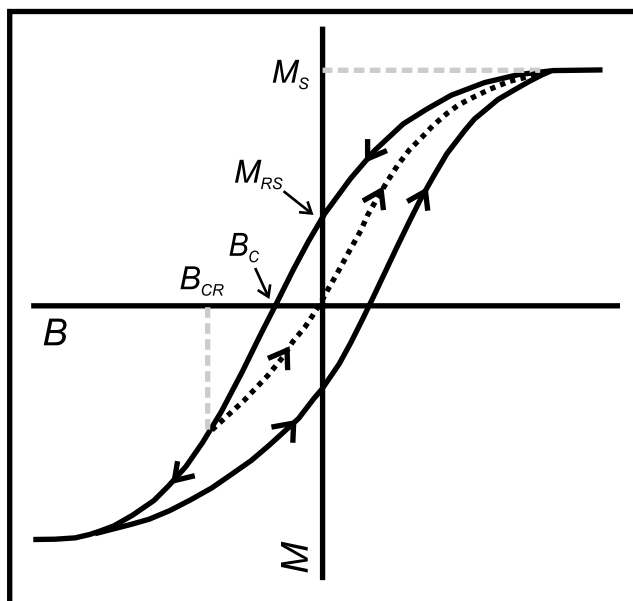


**Figure 3.** Idealized hysteresis loop where  $B$  and  $M$  are the applied and induced magnetic fields, respectively.  $M_S$  is the saturation magnetization,  $M_{RS}$  is the remanent saturation magnetization,  $B_{CR}$  is the coercivity of remanence, and  $B_C$  is the coercivity. A family of minor ascending hysteresis branches could be generated by reversing the field in the positive direction at various points on the major descending branch. Of these minor ascending branches, the one that passes through the origin (dotted line) sets the value of  $B_{CR}$ . In practice,  $B_{CR}$  was determined by demagnetizing  $M_{RS}$ , acquired at 800 mT, with incrementally larger negative magnetic fields until  $M_{RS}$  was reduced to 0.

using the 25–30 samples collected after each experiment. The orientations of the three ellipsoid axes of each sample were projected onto lower hemisphere, equal-area stereonet. Following the method of Mark [1973], eigenvectors  $V_1$ ,  $V_2$ , and  $V_3$  and corresponding normalized eigenvalues  $S_1$ ,  $S_2$ , and  $S_3$  were calculated on the basis of the orientation distribution of  $k_1$ , the maximum AMS principal axis. The  $S_1$  eigenvalue represents the strength of the fabric, or degree of clustering of  $k_1$  orientations around the  $V_1$  eigenvector. An  $S_1$  eigenvalue of 0.33 indicates no alignment of  $k_1$  orientations, whereas an  $S_1$  eigenvalue of 1.0 indicates  $k_1$  orientations that are perfectly aligned.

[17] Rock magnetic experiments were also performed to determine the minerals and grain sizes responsible for the AMS. These experiments were conducted on bulk samples and sieved subsamples of fine-grained (clay and silt < 63  $\mu\text{m}$ ) and coarse-grained (sand and gravel > 63  $\mu\text{m}$ ) sediment. Prior to sieving the bulk sample was deflocculated in order to minimize particle adhesion with clays and among clays. To determine the mineralogy of magnetic particles, samples of both fine (<63  $\mu\text{m}$ ) and coarse (>63  $\mu\text{m}$ ) fractions of the tills were heated from 25 to 700°C and cooled back to 25°C while measuring the bulk magnetic susceptibility using a Geofyzika KLY-3 Kappa-Bridge. Experiments were conducted both in air and argon. The latter minimized heating-induced alterations that were significant in air. At a temperature called the unblocking

temperature, thermal energy will be sufficiently high to destabilize magnetic moments in the weak applied field of the device, causing a reduction in susceptibility. This temperature, which is generally less than and never exceeds the Curie temperature (determined in high saturating magnetic fields), is a good indicator of the mineralogy of magnetic particles. In addition, hysteresis experiments were performed in which a magnetic field  $B$  was applied to the fine and coarse till fractions, gradually increased to a high value, and then gradually decreased in the opposite direction ( $\pm 800$  mT using a 2 Hz vibrating sample magnetometer). Plotting the resultant magnetization as a function of the applied field yields a hysteresis loop (Figure 3). The shape of this loop depends on the mineralogy and sizes of magnetic particles. Several parameters that collectively describe the shape of the loop can be defined on the basis of such data: the saturation magnetization  $M_S$ , the maximum magnetization attainable, the remanent saturated magnetization  $M_{RS}$ , the magnetization under no applied field, the coercivity of remanence  $B_{CR}$ , the reverse applied field required to reduce the remanent saturation magnetization to 0, and the coercivity  $B_C$ , the reverse applied field required to reduce the saturation magnetism to 0 (Figure 3). Commonly the ratio  $M_{RS}/M_S$  is plotted as a function of  $B_{CR}/B_C$  on a so-called Day diagram [e.g., Day *et al.*, 1977; Dunlop, 2002]. These ratios reflect, in part, the number of magnetic domains contained in particles; the number of domains per particle increases predictably with particle size, and hence these ratios can be used to estimate sizes of magnetic particles.

### 3. Results

#### 3.1. Strain Distribution

[18] Locations of strain marker beads excavated at the ends of experiments showed that shear strain was distributed across the central portion of the sample (Figure 4). Depending on the experiment, the thickness of this shear zone ranged from 10 to 30 mm, with an average thickness of 18 mm for the Douglas till and 22 mm for the Batestown

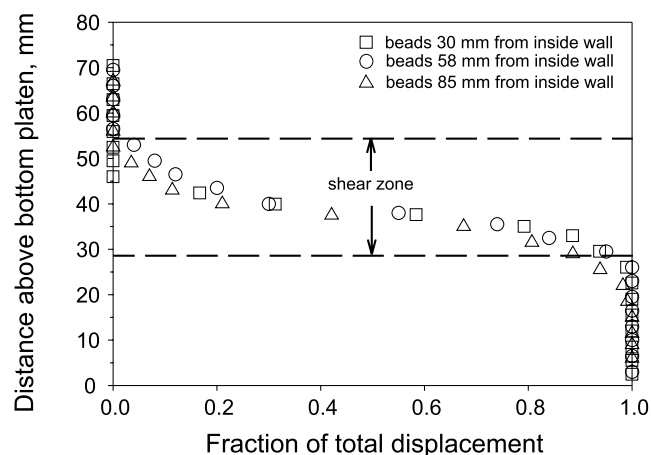


**Figure 4.** The vertical distribution of shearing displacement after an experiment, as determined by the displacement of beads, initially inserted in three vertical columns across the width of the till specimen.

**Table 1.** Parameters Describing Shear Deformation

Experiment	Shearing Displacement at Sample Centerline (mm)	Shear Zone Thickness $h$ (mm)	Shear Strain $\gamma$
<i>Douglas Till</i>			
D-1	100	10	6.3 <sup>a</sup>
D-2	1400	20	70.0
D-3	0	0	0
D-4	2	17.5	0.1
D-5	50	24	2.1
D-6	500	20	25.0
<i>Batestown Till</i>			
B-7	100	21	4.8
B-8	1400	20	70.0
B-9	0	0	0
B-10	50	25	2.0
B-11	500	18	27.8
B-12	2	20	0.1
B-13	20	30	0.7

<sup>a</sup>The shear zone thickness was less than the interior thickness of the AMS sample cube (16 mm), so a depth-averaged shear strain was calculated across this thickness.

till. With the exception of one experiment (D-1), the thickness of sheared till was sufficient to fill the sample boxes for AMS analyses (Table 1; the interior dimension of the boxes was  $\sim 16$  mm). Shear strain was calculated by dividing the total shear displacement at the sample centerline by the centerline shear zone thickness. In the case of experiment D-1, the shear zone was only 10 mm thick, so shear strain was nonuniformly distributed in samples from this experiment. In this case the depth-averaged shear strain within the sample was calculated by dividing the shear displacement across the thickness of the sample by that thickness. Shear strains ranged from 0 (confined consolidation only) to 70 for both tills.

### 3.2. Magnetic Mineralogy and Grain Size

[19] The mean volume susceptibility of the Douglas till ( $834 \pm 150 \mu\text{SI}$ ) is  $\sim 3$  times greater than that of the Batestown till ( $285 \pm 38 \mu\text{SI}$ ) (Table 2). This likely reflects a higher concentration of magnetic minerals derived from the erosion of Precambrian rocks of the Superior basin

compared to the Paleozoic sedimentary rocks of the Michigan basin.

[20] Magnetite dominates the magnetic mineralogy of the two tills, as indicated by the dependence of magnetic susceptibility on temperature (Figure 5), although the Douglas till also contains hematite. For the fine and coarse fractions of both tills there were abrupt reductions in susceptibility at temperatures of  $\sim 590$ – $600^\circ\text{C}$ . These unblocking temperatures are indicative of magnetite and roughly equal to its Curie temperature. However, if the reduction in susceptibility at high temperatures is analyzed in detail for the fine fraction of the Douglas till using the graphical method of *Grommé et al.* [1969], additional unblocking becomes apparent at about  $675^\circ\text{C}$  (see inset in Figure 5b). This unblocking is best attributed to hematite in the Douglas till, in agreement with its red color. If this hematite unblocking is also present in the coarse fraction, its hematite concentration is too low to be detected over the dominant signal of the magnetite.

[21] Hysteresis loop parameters for the bulk, fine, and coarse fractions of the tills provide an additional means of evaluating the magnetic mineralogy. The saturation magnetization  $M_S$  is about 4 times and 10 times the remanent saturation magnetism  $M_{RS}$  for the Douglas and Batestown tills, respectively (Figure 6; Table 3). Using an  $M_S$  value of  $92.4 \text{ Am}^2/\text{kg}$  for magnetite [Dunlop and Özdemir, 1997], the minimum ferrimagnetic content by mass was determined to be 0.14% for the Douglas till and 0.04% for the Batestown till. This observation is consistent with the large difference in the volume susceptibilities of the two tills (Table 2), and confirms that the concentration of magnetic minerals is greater in the Douglas till than in the Batestown till. In addition, the presence of hematite in the Douglas till is suggested by its higher coercivity ( $B_C$ ) and coercivity of remanence ( $B_{CR}$ ) (Table 3); hematite has a coercivity roughly 1 order of magnitude greater than that of magnetite [Dunlop and Özdemir, 1997].

[22] The dependence of magnetic susceptibility on temperature provides some information about sizes of magnetic grains. For both size fractions of the Batestown till, there is a marked peak in susceptibility at  $500^\circ\text{C}$  (Figure 5a). This peak (the so-called Hopkinson effect) is most pronounced in

**Table 2.** AMS Data From Experiments (Ordered by Shear Strain)

Experiment	$n$	Normal Stress (kPa)	Shear Strain	$K_v^a$ ( $\mu\text{SI}$ )	$K_1^a$ ( $\mu\text{SI}$ )	$K_2^a$ ( $\mu\text{SI}$ )	$K_3^a$ ( $\mu\text{SI}$ )	$P_j^a$	$T_j^a$	$P\%^a$ (%)
<i>Douglas Till</i>										
D-3	25	65	0.0	$875 \pm 202$	$892 \pm 207$	$875 \pm 204$	$858 \pm 194$	$1.040 \pm 0.015$	$-0.04 \pm 0.42$	$3.8 \pm 1.4$
D-4	25	65	0.1	$816 \pm 101$	$836 \pm 99$	$816 \pm 103$	$798 \pm 101$	$1.051 \pm 0.018$	$-0.02 \pm 0.48$	$4.8 \pm 1.7$
D-5	25	65	2.1	$793 \pm 64$	$811 \pm 66$	$797 \pm 64$	$773 \pm 65$	$1.053 \pm 0.014$	$0.24 \pm 0.39$	$4.8 \pm 1.3$
D-1	25	65	6.3	$810 \pm 282$	$828 \pm 291$	$811 \pm 279$	$791 \pm 277$	$1.047 \pm 0.016$	$0.21 \pm 0.34$	$4.5 \pm 1.5$
D-6	25	65	25.0	$859 \pm 116$	$880 \pm 117$	$879 \pm 117$	$859 \pm 116$	$1.051 \pm 0.009$	$-0.04 \pm 0.32$	$4.9 \pm 0.9$
D-2	27	65	70.0	$849 \pm 135$	$868 \pm 132$	$849 \pm 133$	$829 \pm 134$	$1.049 \pm 0.015$	$0.07 \pm 0.35$	$4.7 \pm 1.4$
<i>Batestown Till</i>										
B-9	25	65	0.0	$285 \pm 30$	$294 \pm 32$	$286 \pm 31$	$275 \pm 27$	$1.070 \pm 0.037$	$0.11 \pm 0.46$	$6.5 \pm 3.1$
B-12	25	65	0.1	$246 \pm 19$	$252 \pm 20$	$245 \pm 19$	$240 \pm 18$	$1.049 \pm 0.019$	$-0.06 \pm 0.73$	$4.7 \pm 1.6$
B-13	25	65	0.7	$259 \pm 63$	$267 \pm 66$	$259 \pm 64$	$251 \pm 58$	$1.062 \pm 0.022$	$-0.05 \pm 0.43$	$5.9 \pm 1.9$
B-10	25	65	2.0	$297 \pm 29$	$306 \pm 31$	$296 \pm 30$	$289 \pm 27$	$1.060 \pm 0.024$	$-0.23 \pm 0.40$	$5.6 \pm 2.2$
B-7	30	65	64.8	$309 \pm 74$	$316 \pm 78$	$309 \pm 73$	$300 \pm 72$	$1.055 \pm 0.014$	$0.17 \pm 0.37$	$5.2 \pm 1.3$
B-11	25	65	27.8	$300 \pm 18$	$309 \pm 18$	$299 \pm 18$	$291 \pm 18$	$1.062 \pm 0.013$	$-0.16 \pm 0.18$	$5.9 \pm 1.3$
B-8	25	65	70.0	$297 \pm 36$	$307 \pm 40$	$295 \pm 34$	$284 \pm 33$	$1.066 \pm 0.030$	$-0.31 \pm 0.38$	$6.2 \pm 2.7$

<sup>a</sup>Values represent the mean and  $\pm 1$  standard deviation.

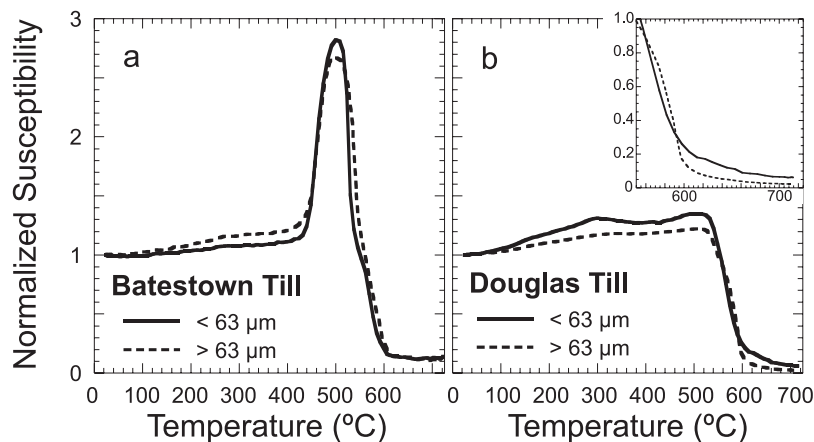


**Figure 5.** Magnetic susceptibility, normalized to susceptibility at 25°C, during heating of the coarse and fine fractions of the (a) Batestown till and (b) Douglas till. The inset diagram Figure 5b shows the detail of the data between 550 and 725°C. Coarse and fine fractions of both tills were separated by mechanical sieving.

very small single-domain magnetite particles ( $<0.1 \mu\text{m}$ ) that become highly susceptible to magnetization at temperatures that are high but below the Curie temperature [Dunlop and Özdemir, 1997]. The Hopkinson effect indicates that some magnetic grains of the Batestown till are smaller than  $0.1 \mu\text{m}$ , and the Hopkinson peak for both size fractions indicates that larger rock particles contain many of these grains. The lack of a Hopkinson peak in the experiments on the Douglas till indicates that it does not contain this extremely fine-grained magnetite.

[23] More complete information regarding average sizes of magnetic grains is provided by hysteresis loop parameters and particularly the ratios  $M_{RS}/M_S$  and  $B_{CR}/B_C$ , although caution should be applied because  $M_{RS}$  and  $B_{CR}$  are not intrinsic properties of a given mineral and can vary for a single grain size depending on internal deformation of grains [see Dunlop, 2002]. Values of these ratios for the Batestown till indicate a mean magnetite grain size of  $\sim 15 \mu\text{m}$  [see Dunlop, 2002, Figures 8c, 8d, and 8e], within the so-called pseudo single domain range in which there are probably several magnetic domains within a particle ( $0.5 > M_{RS}/M_S > 0.02$ ,  $2 < B_{CR}/B_C < 5$ ). Given that  $15 \mu\text{m}$  is the mean magnetite particle size in the Batestown till and that a much finer ( $<0.1 \mu\text{m}$ ) single domain fraction is indicated by the Hopkinson effect (Figure 5a), there must also be some magnetite grains somewhat larger than  $15 \mu\text{m}$ . Interpretations are more difficult for the Douglas till, owing to the effect of hematite on the hysteresis loop parameters. In particular, the ratio  $M_{RS}/M_S$  can be skewed upward by single domain hematite ( $0.5\text{--}\sim 15 \mu\text{m}$ ). This effect is probably responsible for values of this ratio being larger for the Douglas till than the Batestown till (Table 3).

[24] Values of the ratios  $M_{RS}/M_S$  and  $B_{CR}/B_C$  are similar for both the coarse and fine fractions, indicating that most magnetite grains are contained as inclusions within larger single-mineral or multimineral particles (rock fragments). The measured values of  $M_S$  for bulk, coarse, and fine samples (Table 3) can be used to estimate a minimum value for the mass fraction of magnetite grains  $m$  included in other minerals or rock fragments. Values of  $M_S$  are independent of grain size and linearly additive. If we assume that all

magnetite particles of the coarse fraction consist of inclusions, which is a good approximation because the mean magnetite grain size is  $\sim 15 \mu\text{m}$ , and assume that none of the fine fraction contains magnetite inclusions, which is clearly an underestimate, then

$$M_{SB} = mM_{SC} + M_{SF}(1 - m), \quad (4)$$

where  $M_{SB}$ ,  $M_{SC}$ , and  $M_{SF}$  are values of  $M_S$  for the bulk, coarse, and fine samples, respectively (Table 3). Solving for  $m$  in this equation yields  $m = 0.59$  for the Douglas till and  $m = 0.50$  for the Batestown till. These are minimum values for the mass fraction of magnetite grains in larger particles

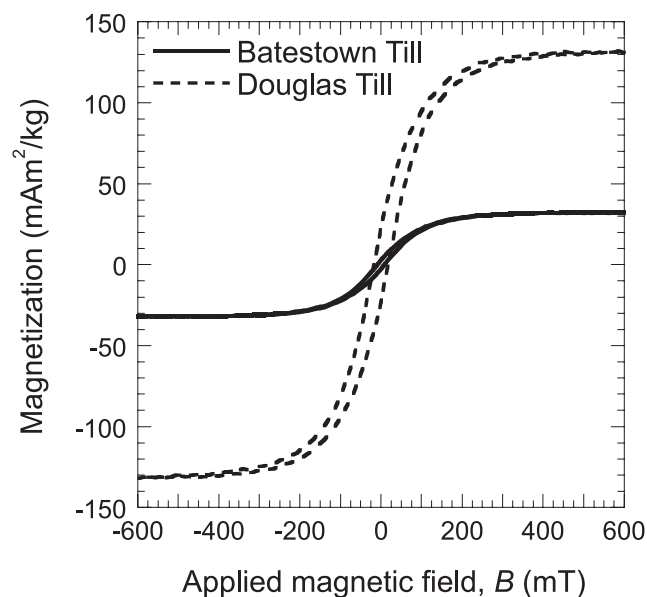


**Figure 6.** Hysteresis loops of representative samples of the Batestown and Douglas tills (high-field paramagnetic and diamagnetic contributions have been removed). The hysteresis parameters deduced from these loops (see Figure 3) for the bulk sample and for fine and coarse fractions are listed in Table 3.

**Table 3.** Hysteresis Loop Parameters for the Bulk, Fine (<63  $\mu\text{m}$ ), and Coarse (>63  $\mu\text{m}$ ) Fractions of the Douglas and Batetown Tills

	$M_{RS}$ ( $\text{Am}^2/\text{kg}$ )	$M_S$ ( $\text{Am}^2/\text{kg}$ )	$B_C$ (mT)	$B_{CR}$ (mT)	$M_{RS}/M_S$	$B_{CR}/B_C$
<i>Douglas Till</i>						
Bulk	0.0215	0.131	16.7	45.1	0.164	2.70
Fine	0.0265	0.148	19.2	49.7	0.179	2.59
Coarse	0.0205	0.119	15.7	44.5	0.172	2.82
<i>Batetown Till</i>						
Bulk	0.0020	0.031	8.90	32.9	0.064	3.70
Fine	0.0030	0.035	9.15	33.4	0.086	3.65
Coarse	0.0020	0.027	9.45	34.3	0.074	3.63

because many such particles will be part of the fine fraction (<63  $\mu\text{m}$ ).

[25] Overall, the susceptibility versus temperature data and hysteresis experiments provide three important conclusions: magnetite is the principal magnetic mineral in each till (although the Douglas till contains some hematite), magnetic grains are generally silt sized or smaller, and most magnetic grains (>50–59% by mass) are contained as inclusions within larger single-mineral or multimineral rock particles.

### 3.3. Anisotropy of Magnetic Susceptibility

[26] The magnetic anisotropy, as determined from the principal susceptibilities of individual samples, was small and did not vary systematically with shear strain magnitude. AMS ellipsoids were close to being spheres. Average percent anisotropy for samples from all experiments was  $4.6 \pm 1.4\%$  for the Douglas till and  $5.7 \pm 2.0\%$  for the Batetown till. Similarly, mean values of the shape parameter and the corrected degree of anisotropy were near 0 and 1.0, respectively (Table 2). Plotting mean values of these two parameters as a function of shear strain magnitude yielded no clear pattern of variability with strain (Figure 7).

[27] In contrast, the fabric formed by the orientations of AMS ellipsoids did change significantly and systematically with strain (Figure 8). Some alignment of  $k_1$  orientations occurred during consolidation of the tills prior to shearing, as indicated by initial  $S_1$  eigenvalues of  $\sim 0.5$  (Table 4). During the early stages of deformation (up to shear strains of  $\sim 6$ )  $S_1$  eigenvalues increased rapidly to values of 0.73–0.77. By shear strains of  $\sim 25$ ,  $S_1$  eigenvalues were  $\sim 0.94$  and did not increase with further strain. The regressions of  $S_1$  on shear strain for the two tills are similar. However, after the experiment with the Douglas till conducted to the highest strain (70), there was a reduction in fabric strength to 0.83 (Figure 8a). Although this value lies just outside the standard error of the regression (0.063), the significance of this fabric reduction cannot be evaluated without a second suite of experiments conducted to very high strains. Also, if  $S_1$  eigenvalues are plotted against  $S_3$  eigenvalues (Figure 9), the tendency for  $S_3$  to decrease with strain is apparent, although that decrease is not as systematic as the increase in  $S_1$  with strain.

[28] The orientations of principal susceptibilities plotted on lower hemisphere stereonet depict AMS fabric development in more detail (Figure 8). Weak, relatively symmetric  $k_1$  girdle fabrics (grains weakly aligned with the

horizontal plane) resulted from consolidation, as expected from grain rotation caused by this process. Up to shear strains of  $\sim 6$ , these girdle fabrics strengthened by becoming increasingly asymmetric, with  $k_1$  orientations increasing their alignment with the plane of shearing and  $k_3$  orientations tending to cluster with a steep “down-glacier” plunge. At shear strains of  $\geq 25$ ,  $k_1$  orientations became tightly clustered in the direction of shear and plunged “up-glacier,” at angles of 18 and 26° for the Douglas and Batetown tills, respectively. In the experiment conducted to the highest strain with the Douglas till (Figure 8a), 3 of the 27 samples had  $k_1$  orientations well outside this flow-parallel cluster, which explains the reduction in  $S_1$  that occurred in that experiment. The orientations of  $V_1$  eigenvectors at various strains clearly illustrate the rotation of ellipsoid long axes toward the direction of shear with strain (Figure 10). At these highest strains  $k_2$  orientations were nearly parallel to the shear plane and transverse to the direction of shear, and

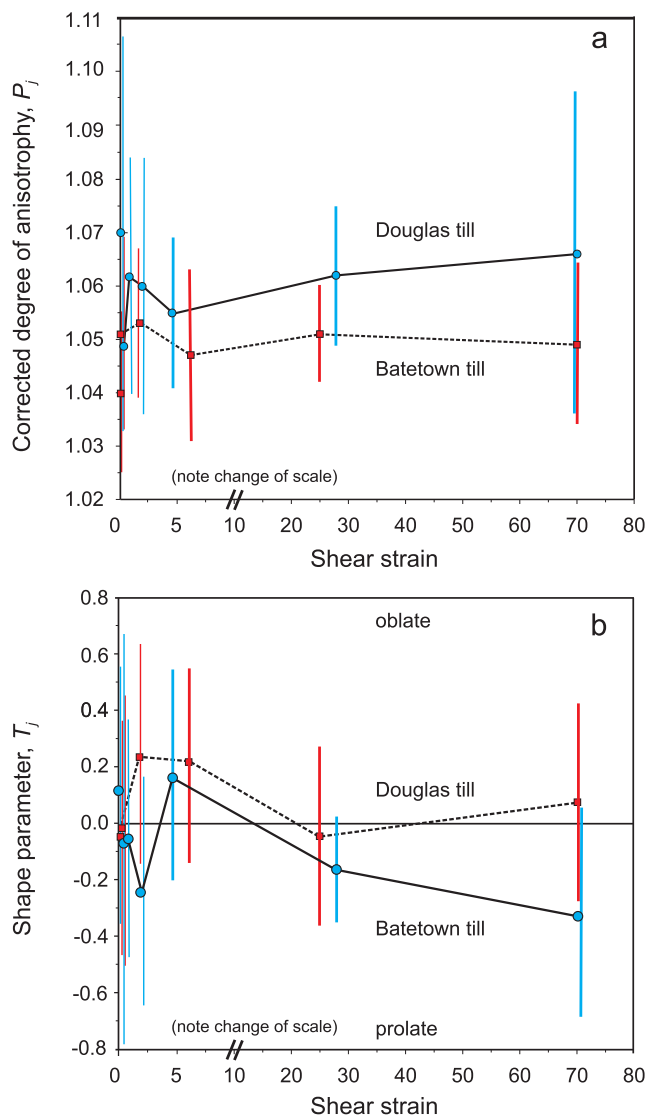


**Figure 7.** (a) Corrected degree of anisotropy and (b) shape parameter as a function of shear strain for the Batetown and Douglas tills. Error bars indicate  $\pm 1$  standard deviation.

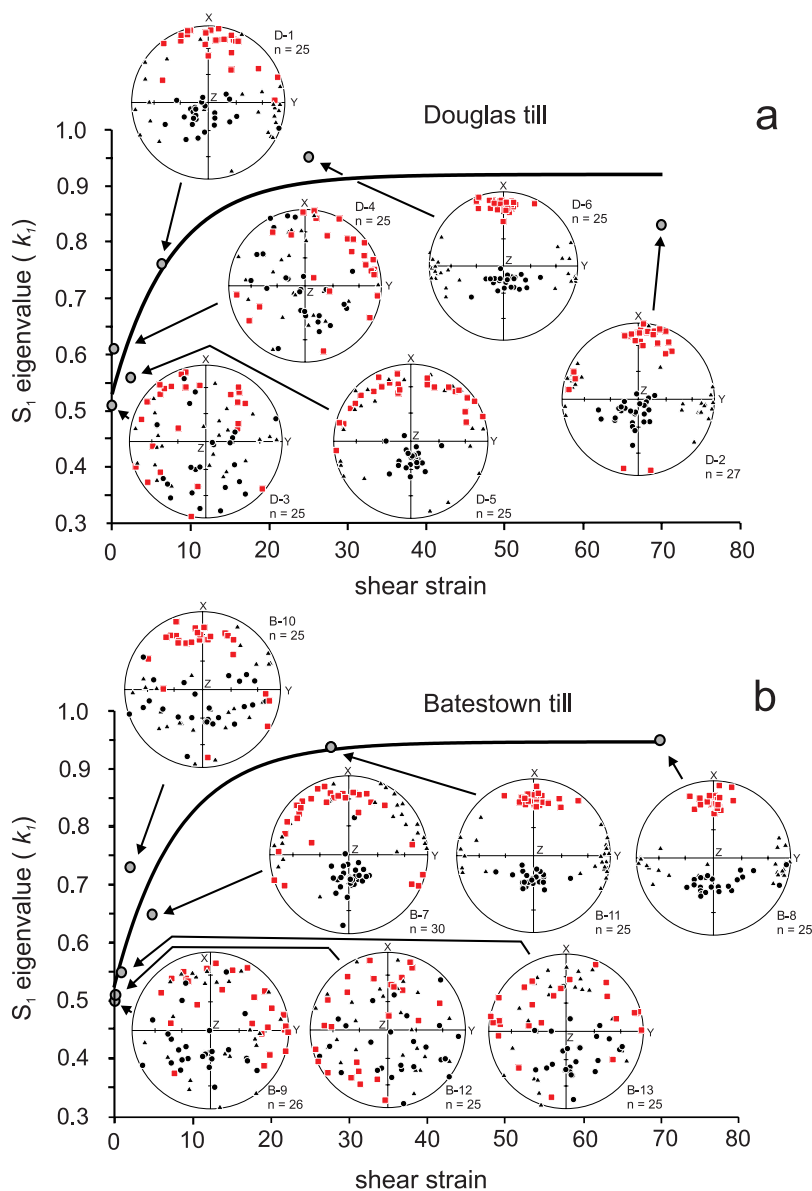


**Figure 8.** AMS fabric strength, based on  $k_1$  orientations, as a function of shear strain for the (a) Douglas till and (b) Batestown till. Lines of the form  $y = y_0 + a(1 - e^{-bx})$  were fitted to the data. Standard errors were 0.063 and 0.067 for the Douglas and Batestown tills, respectively. Lower hemisphere stereonet accompany each data point showing the maximum (squares), intermediate (triangles), and minimum (circles) principal susceptibilities. The direction of shearing is along the x axis and the sense of shearing in the stereonet is bottom north and top south. Stereonet labels indicate experiment number and the number of samples ( $n$ ).

orientations of  $k_3$  plunged steeply down-glacier, tending to be symmetrically distributed about the direction of shear (Figure 8).

## 4. Discussion

### 4.1. Laboratory Results

[29] Our finding that the magnetic mineralogy of both tills is dominated by magnetite explains why the AMS of these tills provides information about strain magnitude. Two factors contribute to the AMS of rocks and sediments. Crystalline anisotropy results from lattice forces of a magnetic mineral affecting electron spin configuration within its

grains, so that magnetization acquired in an applied field depends on the crystallographic orientation. Shape anisotropy, on the other hand, is a consequence of an internal demagnetization field created by apparent magnetic charges on the grain surface in the presence of an external applied field. In most nonequant particles this results in magnetization that is preferentially induced along the long axis of a grain. AMS associated with magnetite is dominated by shape anisotropy, so it is the rotation of nonequant magnetite grains with strain that is responsible for the AMS of the till. In contrast, in hematite, for example, crystalline anisotropy is dominant [e.g., *Tarling and Hrouda, 1993*].

**Table 4.** AMS Fabric Data

Sample Group	n	Shear Strain	Eigenvector $V_1$ (°)						Eigenvector $V_3$ (°)					
			$S_1$	$S_2$	$S_3$	Trend	Plunge	95% Confidence Ellipse		Trend	Plunge	95% Confidence Ellipse		
								Maximum Angle	Minimum Angle			Maximum Angle	Minimum Angle	
<i>Douglas Till</i>														
D-3	25	0.0	0.51	0.35	0.14	350	21	48.1	14.2	174	69	26.6	14.1	
D-4	25	0.1	0.61	0.27	0.12	55	12	25.2	10.1	201	76	22.0	10.0	
D-5	25	2.1	0.56	0.43	0.01	3	22	55.1	4.8	177	67	5.0	4.7	
D-1	25	6.3	0.77	0.19	0.04	5	16	14.2	5.7	210	73	18.9	5.8	
D-6	25	25.0	0.95	0.04	0.01	359	18	5.8	3.6	221	67	34.8	3.4	
D-2	27	70	0.83	0.14	0.03	6	14	7.5	4.9	165	75	9.4	4.9	
<i>Batestown Till</i>														
B-9	26	0.0	0.50	0.40	0.10	83	13	54.7	13.6	195	58	15.5	13.6	
B-12	25	0.1	0.50	0.34	0.16	25	10	45.4	20.7	127	49	29.3	20.7	
B-13	25	0.7	0.55	0.34	0.11	273	9	34.2	12.6	170	53	20.3	12.6	
B-10	25	2.0	0.73	0.21	0.06	348	28	15.6	7.0	197	59	18.5	6.3	
B-7	30	4.8	0.65	0.31	0.04	327	21	24.6	5.6	183	65	10.2	5.3	
B-11	25	27.8	0.94	0.05	0.01	3	26	5.8	3.1	177	64	19.7	3.0	
B-8	25	70	0.96	0.02	0.02	1	28	4.6	4.3	99	15	75.5	4.3	

[30] An important result of this study is that the magnitude of anisotropy of a given sample, as indicated by the percent total anisotropy, the shape parameter, and the corrected degree of anisotropy, does not vary systematically with strain magnitude (Figure 7), whereas the fabric formed by  $k_1$  orientations progressively strengthens with strain (Figure 8). Or put differently, AMS ellipsoids remain close to spherical as strain progresses, but the degree of alignment of these ellipsoids increases conspicuously. The high sphericity of ellipsoids is because most magnetite particles, which are silt sized or smaller, are contained within larger rock particles: a conclusion supported by both the small difference in hysteresis parameters for the fine and coarse fractions of the tills (Table 3) and the calculated minimum values for the mass fraction of magnetite inclusions in larger grains (0.50–0.59). As a result, the shape anisotropy of most magnetic grains does not contribute to the magnitude of anisotropy of sheared till because, although larger grains rotate during shear, magnetic grains are not oriented preferentially within them. This observation explains why our data contradict results of theoretical models of rock deformation that predict systematic increases in the magnitude of anisotropy up to strains of  $\sim 10$  [e.g., Hrouda and Jezek, 1999]: such models do not account for most magnetite grains being contained in larger rock particles. Rotation of only particles small enough to consist mainly of magnetite impart anisotropy to the till as it shears. In our experiments the resulting alignment of only a small fraction of magnetic grains caused AMS ellipsoids to remain nearly spherical but become progressively aligned with strain.

[31] Thus, the fabric development with strain documented in Figure 8 reflects the rotation of silt sized and smaller grains that consist mainly of magnetite. The long axes of these grains underwent some rotation toward horizontal during consolidation. Asymmetric girdle fabrics that developed thereafter at low shear strains (up to  $\sim 6$ ) indicate rotation of these grains toward the plane of shear, with some rotation toward the shearing direction to produce the asymmetry. Between strains of  $\sim 6$  and  $\sim 25$ , the primary effect of

shear was to rotate near-horizontal grains toward the shearing direction, resulting in strong clustering of the orientations of particle long axes. No further increases in particle alignment occurred at strains  $> \sim 25$ .

[32] The AMS fabric development in these experiments is similar to the development of fabric by pebbles [Hooyer and Iverson, 2000a] and sand particles [Thomason and Iverson, 2006] in other experiments conducted with our ring shear device under similar conditions: fabrics strengthened parallel to the shearing direction at an exponentially decreasing rate with strain, and fabric development was complete at strains of 7–35. Also, at the highest strains long axes of sand particles and pebbles plunged slightly up-glacier, as did  $k_1$  orientations in this study (Figures 8 and 10).

[33] There is a temptation to also assign significance to the relative strengths of AMS and particle fabrics, as indicated by the relative magnitudes of  $S_1$  eigenvalues. For example, the strongest AMS fabrics of these experi-

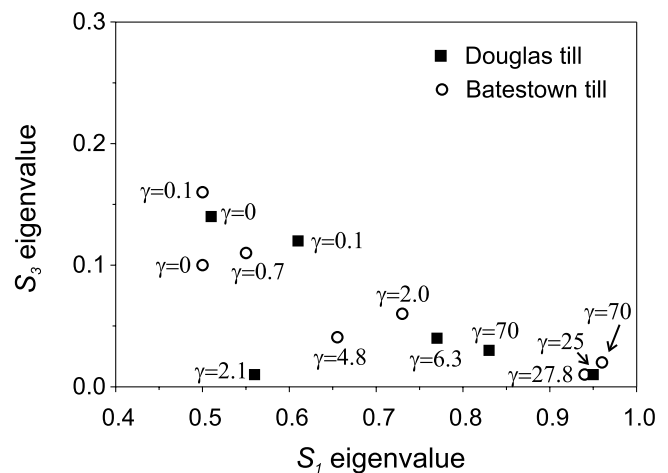


**Figure 9.** Bivariate plot of eigenvalues based on  $k_1$  orientations for experiments with the two tills. The shear strain from each experiment is  $\gamma$ .

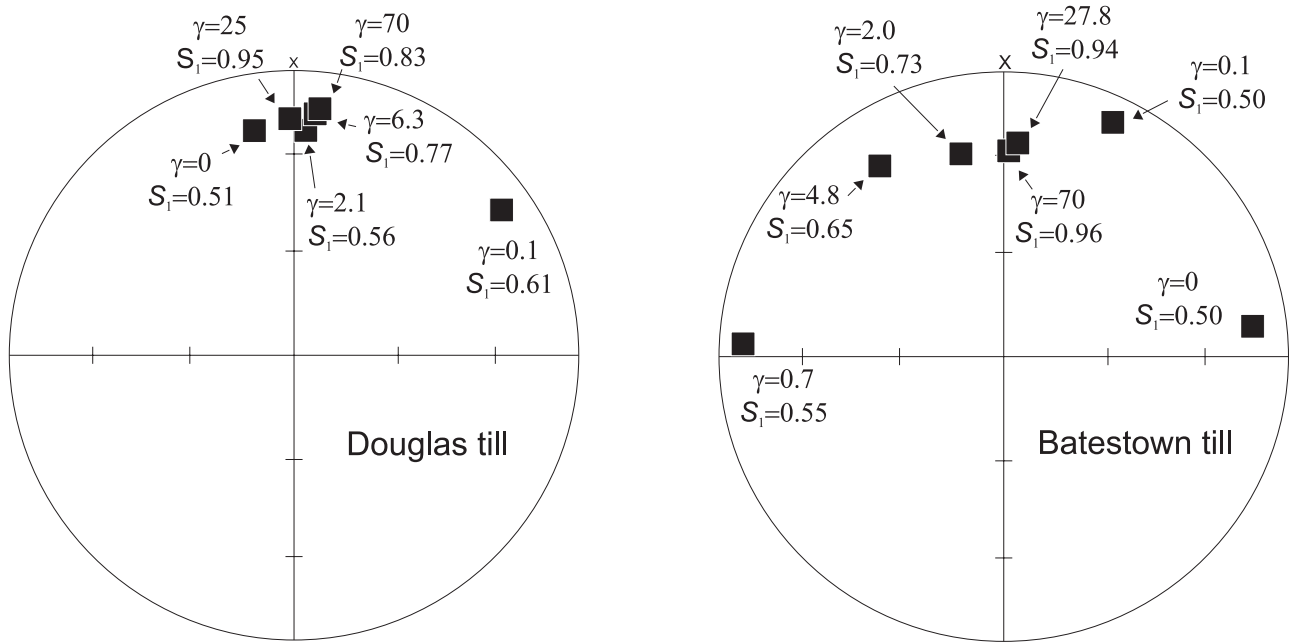


**Figure 10.** Orientation of  $V_1$  eigenvectors for the Douglas and Batestown tills plotted on lower hemisphere stereonets for different values of the corresponding shear strain  $\gamma$  and eigenvalue  $S_1$ . Sense of shear is bottom north and top south.

ments are stronger than pebble or sand-particle fabrics developed at comparable strains [Hooyer and Iverson, 2000a; Thomason and Iverson, 2006]; this observation might appear at face value to contradict evidence that smaller particles develop weaker fabrics than larger particles [Kjær and Krüger, 1998; Carr, 2001; Thomason and Iverson, 2006], given that AMS fabrics reflect rotation of silt-sized and smaller magnetite grains. However, strengths of AMS and particle fabrics cannot be compared in this way. AMS  $k_1$  orientation reflects the volume-averaged alignment of many grains, rather than a single grain, and the magnetic signal associated with this average alignment is affected not only by the physical alignment of the grains but by the nature of their shape or crystalline anisotropy. Thus, assigning significance to the relative magnitudes of  $S_1$  values for AMS and particle fabrics is probably unwise.

[34] Although  $S_1$  values of AMS and particle fabrics cannot be compared directly, fabric evolution and direction are very similar for the two kinds of fabric, implying that some conclusions from earlier experimental studies of particle rotation [Hooyer and Iverson, 2000a; Thomason and Iverson, 2006] apply here also. Foremost among these conclusions is that particles do not obey the Jeffery model of particle rotation [Jeffery, 1922], formulated for the case of elongate particles in a viscous shearing fluid, with no slip of fluid across particle surfaces. In the Jeffery model elongate particles rotate indefinitely through the shear plane, resulting in only weakly aligned particles. Till, however, is not intrinsically viscous [Iverson et al., 1998; Tulaczyk et al., 2000], and more importantly there is slip at particle surfaces. As a result particles rotate into the plane of shearing, parallel to the direction of shear, and tend to remain there, rather than orbiting through the shear plane [Hooyer and Iverson, 2000a]. The up-glacier plunge of particles that develops with sufficient deformation likely

results from the combined effect of movement along two sets of so-called Riedel microshears:  $R_1$  shears that dip very gently down-glacier and rotate particles near the macroscopic plane of shearing and antithetic  $R_2$  shears that dip steeply down-glacier and rotate particles so that they ultimately plunge slightly up-glacier (Figure 11). Such micros shears have been observed in petrographic thin sections of till sheared in the laboratory [Larsen et al., 2006], including the Douglas till [Thomason and Iverson, 2006], and in field studies of fault gouge [Cladouhos, 1999]. Time-integrated rotation of particles along these micros shears results in strong fabric in the direction of shearing that is slightly

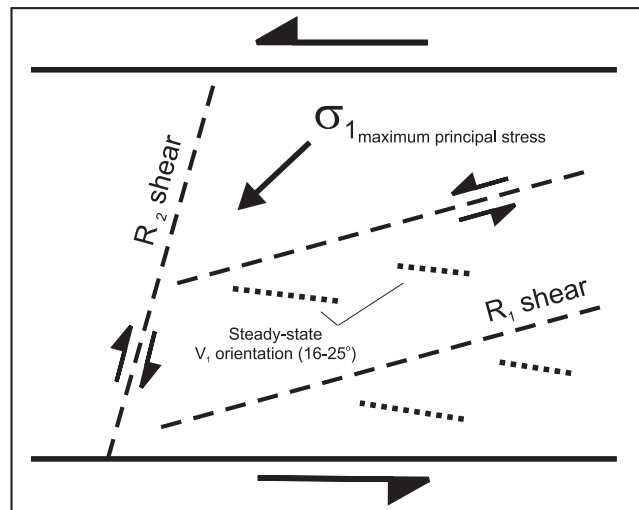


**Figure 11.** Schematic of Riedel shear orientations (dashed lines) and the measured range of steady state  $V_1$  directions (dotted lines). Small arrows show sense of movement along micros shears.

inclined to the shear plane. Also, in no experimental studies with till have transverse particle fabrics developed at high strains, contrary to the original minimum energy postulate of *Jeffery* [1922] and some subsequent interpretations of transverse fabrics in till [e.g., *Hart*, 1994; *Carr and Rose*, 2003]. Thus, the slight fabric weakening caused by the transverse  $k_1$  orientations of 3 of 27 samples collected after the highest strain experiment with the Douglas till (Figure 8a) is likely not significant, particularly because the Batestown till displayed no similar transverse  $k_1$  orientations. However, only more experiments with the Douglas till, conducted to higher strains than those of these experiments, will resolve this issue with certainty.

[35] An important consideration in any experimental study is whether the boundary conditions of the experiment have adversely affected the results. In experiments with our ring shear device, strain is not uniformly distributed in the till specimen, owing to the effect of the upper and lower walls of the sample chamber that focus strain in a shear zone centered on the sliding interface between these walls (Figure 4). We thus make no claim that with these experiments that we are “simulating” deformation of a till layer beneath a glacier, which is probably impossible in a laboratory experiment. Fortunately, our objective has been more modest: to relate AMS fabric to strain magnitude. Thus, because we can readily measure the displacement gradient across our till samples of known thickness, the distribution of strain outside the depth range of sampling is not relevant.

[36] More relevant is whether AMS fabrics might be affected by variables kept constant in these experiments, most notably the shear rate and effective normal stress on the specimen. Although more experiments are planned to explore the possible effects of these variables on AMS fabric development, related experimental results provide guidance for estimating these effects. Tills and other granular materials, if sheared to their so-called critical state, attain a steady shear strength, called the residual or ultimate strength, that depends on the fabric formed by fine particles [e.g., *Skempton*, 1985]. This residual strength is only very weakly dependent on shear rate over a range of glacial (noninertial) rates [e.g., *Tika et al.*, 1996]. This lack of dependence of residual strength on shear rate has been demonstrated for tills [*Iverson et al.*, 1998] and implies that the AMS fabric formed by fine magnetite grains will also be only weakly dependent on shear rate. Effective normal stress affects the critical state porosity of granular materials, which in turn could affect the rotation and alignment of silt-sized magnetite particles. However, even for virgin consolidation in the absence of shear, the porosity of a fine-grained till (from beneath Whillans Ice Stream) is reduced in response to a 100-fold increase in effective normal stress (5–500 kPa [*Tulaczyk et al.*, 2000]) by only ~30%. In contrast, shear strain may vary through several orders of magnitude. A reasonable conjecture, therefore, is that the role of effective stress variations is subordinate to that of shear strain magnitude in controlling AMS fabric development.

#### 4.2. Application to Field Studies

[37] Empirical evidence for connecting fabric characteristics of glacial diamictons to specific depositional facies

[e.g., *Hart*, 1994; *Hicock et al.*, 1996] is not convincing [*Bennett et al.*, 1999], and the physical rationale for making such connections is unclear, given that the origins of most subglacial facies involve some shear deformation of either dirty basal ice or a soft bed. We thus confine this discussion to how our laboratory results can be applied to estimate strain magnitude in basal tills of the geologic record and how these estimates could be applied in testing the bed deformation model of glacier flow and sediment transport.

[38] Deformation of both tills to moderate strains (~25) yielded strong  $k_1$  fabrics ( $S_1 = 0.83$ – $0.95$  for the Douglas till;  $S_1 = 0.94$ – $0.96$  for the Batestown till). Thus, provided that no postglacial disturbance of fabric has occurred and subglacial deformation consisted mostly of simple shear, intact samples of these tills with  $S_1$  eigenvalues that fall well below these ranges can be interpreted as contradicting the bed deformation hypothesis, which normally will require strains much >25. In addition,  $k_1$  orientations formed asymmetric girdle fabrics at strains <~6 but became tightly clustered parallel to shearing direction at a strain of ~25. Thus, with the same caveat that simple shear is dominant, symmetric or asymmetric girdle fabrics are also not consistent with the high strains required of the bed deformation model.

[39] Interpretations of strong flow-parallel fabrics are less straightforward. In this case only small strains can be ruled out, owing to the lack of continued fabric development at strains >~25. Moderate strains cannot, therefore, be distinguished from the higher strains required of the bed deformation model. In addition, strong AMS fabrics might conceivably develop by at least three other processes: shear of sediment-laden basal ice, flow of water in a thin layer at the ice-bed interface, and plowing of particles through the bed surface during lodgment. Strong pebble fabrics have been observed in basal ice [*Lawson*, 1979; *Ham and Mickelson*, 1994; *Bennett et al.*, 1999] and the preservation of these fabrics has been documented beneath some glaciers [*Lawson*, 1979; *Ham and Mickelson*, 1994]. The silt-sized and smaller magnetite particles that dictate AMS may become similarly aligned in basal ice, with this fabric preserved upon deposition. In addition, silt-sized and smaller particles would be readily transported by the water film that divides wet-based glaciers from their soft beds. This flow, particularly in a layer sufficiently thin to enable laminar flow, would orient elongate silt particles as they melt out of basal ice and become incorporated in the till bed. Finally, as lodgment till is plastered onto a soft bed, particles plow through the bed surface, causing deformation of the uppermost portion of the bed that can align smaller neighboring particles [*Clark and Hansel*, 1989]. Through this process of bed accretion and strain focused near the glacier sole, a till layer with a uniformly strong fabric throughout its depth could form, even though at any one time the bed never deformed pervasively at depth [*Larsen et al.*, 2004; *Thomason and Iverson*, 2006].

[40] Thus, strong AMS fabrics do not demonstrate that the bed deformation model is correct, but weak fabrics provide evidence against the model. We acknowledge that weak measured fabrics could arise from strain localized in till sufficiently that the sampling density is inadequate to resolve resultant, locally strong fabrics. However, in the bed deformation model as advanced by most authors [e.g.,

Boulton and Hindmarsh, 1987; Alley, 1991; Jenson et al., 1995] strain is assumed to be pervasive, so measured weak fabrics, despite local deformation, would constitute evidence against the bed deformation model.

[41] An important consideration in applying the AMS fabric results of Figures 8–10 to field studies is whether these results can be applied to other tills. Although the forms of the  $S_1$  strain regressions are quite similar for the two tills (Figure 8), they are not identical. In addition, although the AMS of the Douglas and Batestown tills is controlled largely by magnetite, this may not be true of all tills. Tills with other dominant magnetic minerals that have different shape or crystalline anisotropy than magnetite may yield somewhat different results. Thus, this method should be applied with caution to tills with magnetic fabrics that have not been calibrated to strain in the laboratory.

[42] Our study also helps set the spatial resolution of this technique for inferring strain magnitude. The AMS technique provides spatial resolution considerably better than pebble fabric but worse than sand particle fabric. Unfortunately, the magnitude of anisotropy, which can be determined from a single 18 mm cubic specimen, does not provide an indication of strain magnitude (Figure 7). The fabric formed by  $k_1$  orientations, which is a good proxy for strain magnitude, requires multiple specimens (>25 in this study) to be statistically reliable. Thus, this method requires sampling a horizon over a thickness of at least 16 mm and area of  $\sim 0.01$  m<sup>2</sup>. Sand grain fabrics can be measured from thin sections over areas that are smaller.

[43] However, the advantages of AMS fabric determinations outweigh their disadvantages. Three-dimensional fabrics can be determined rapidly and cheaply, without the need to impregnate intact specimens with epoxy and prepare thin sections. Perhaps more importantly, the only human error involves recording the orientations of AMS samples. This can be done on a horizontal platform excavated in an outcrop with far less subjectivity than the measurement of irregularly shaped particles. Moreover, each  $k_1$  determination reflects the volume-averaged effect of many particles, rather than the orientation of a single grain, indicating that there will be less inherent variability (noise) in  $k_1$  orientations than in the orientations of single grains. We do not wish to imply that other methods of fabric analysis do not have merit in some contexts, only that the speed, objectivity, and signal-to-noise ratio of AMS fabric determinations exceed those of other methods that we have used [e.g., Hooyer and Iverson, 2000a; Thomason and Iverson, 2006].

## 5. Conclusions

[44] These experiments provide the first calibration of the magnetic properties of tills to the magnitude and direction of shear deformation. Directions of maximum susceptibility ( $k_1$ ) from multiple samples rotate toward the plane of shearing at low shear strains (<6) and cluster strongly in the direction of shear at moderate strains ( $\sim 25$ ), plunging mildly up-glacier.  $S_1$  eigenvalues attained at these and higher strains are 0.83–0.95 for the Douglas till and 0.94–0.96 for the Batestown till. Orientations of  $k_1$  are controlled by the shape anisotropy of nonequant magnetite grains that are silt sized or smaller. Rotation of the long axes of these grains toward the shear plane, with clustering in the

direction of shear, accounts for the AMS fabric. The rate and character of this fabric development is essentially the same as that observed for larger sand and pebble grains, although little insight can be gained from comparing strengths ( $S_1$  values) of AMS fabrics with those of particle fabrics.

[45] Most magnetite grains are contained as inclusions within larger particles and are not preferentially oriented, such that rotation of these larger particles does not contribute to AMS. Thus, the magnitude of anisotropy is too small relative to its variability among samples to resolve a systematic relationship between the magnitudes of anisotropy and shear strain.

[46] Weak AMS fabrics can be used to help identify tills in the geologic record that have been sheared to strains too small to be consistent with the bed deformation model ( $< \sim 6$ – $25$  for the two tills studied here). Stronger flow-parallel fabrics distributed over the thickness of a till unit would imply either that the bed has been sheared pervasively to higher strains or that another process oriented silt-sized magnetite particles during deposition of till from ice. Two such processes might be transport of particles in the melt film at the ice-till interface or local bed deformation due to plowing of grains through the bed surface during progressive accretion of till to the bed. Owing to its speed, lack of subjectivity, and volume averaging of the effects of many particles, AMS determination should be considered for many applications as the preferred method of till-fabric analysis when sufficient analytical facilities are available.

[47] **Acknowledgments.** We thank the U.S. National Science Foundation (OPP136006) for supporting this research and the Institute for Rock Magnetism (IRM) at the University of Minnesota for providing the facilities to gather the magnetic data; Mike Jackson of the IRM was particularly helpful. We also thank Mike Church and two anonymous reviewers whose comments improved the manuscript.

## References

- Alley, R. B. (1991), Deforming-bed origin for southern Laurentide till sheets?, *J. Glaciol.*, *37*, 67–76.
- Alley, R. B. (2000), Continuity comes first: Recent progress in understanding subglacial deformation, *Geol. Soc. Spec. Publ.*, *176*, 171–180.
- Arch, J., J. Maltman, and R. J. Knipe (1987), Shear-zone geometries in experimentally deformed clays: The influence of water content, strain rate and primary fabric, *J. Struct. Geol.*, *10*, 91–99.
- Benn, D. I. (1995), Fabric signature of till deformation, Breidamerkurjokull, Iceland, *Sedimentology*, *42*, 735–747.
- Benn, D. I., and D. J. A. Evans (1996), The interpretation and classification of subglacially-deformed materials, *Quat. Sci. Rev.*, *15*, 23–52.
- Bennett, M. R., R. I. Waller, N. F. Glasser, M. J. Hambrey, and D. Huddart (1999), Glacigenic clast fabrics: Genetic fingerprint or wishful thinking?, *J. Quat. Sci.*, *14*, 125–135.
- Borradaile, G. J. (1991), Correlation of strain with anisotropy of magnetic susceptibility (AMS), *Pure Appl. Geophys.*, *135*, 15–29.
- Borradaile, G. J., and C. Alford (1987), Relationship between magnetic susceptibility and strain in laboratory experiments, *Tectonophysics*, *133*, 121–135.
- Borradaile, G. J., and C. Alford (1988), Experimental shear zones and magnetic fabrics, *J. Struct. Geol.*, *10*, 895–904.
- Borradaile, G. J. and M. Jackson (2004), Anisotropy of magnetic susceptibility (AMS): Magnetic petrofabrics of deformed rocks, in *Magnetic Fabric: Methods and Applications*, *Geol. Soc. Publ.*, *238*, 299–360.
- Borradaile, G. J., and M. A. Puumala (1989), Synthetic magnetic fabrics in plasticine, *Tectonophysics*, *164*, 73–78.
- Boulton, G. S. (1996), The origin of till sequences by subglacial sediment deformation beneath mid-latitude ice sheets, *Ann. Glaciol.*, *22*, 75–84.
- Boulton, G. S., and R. C. A. Hindmarsh (1987), Sediment deformation beneath glaciers: Rheology and geological consequences, *J. Geophys. Res.*, *92*(B9), 9059–9082.

- Carr, S. (2001), Micromorphological criteria for discriminating subglacial and glaciomarine sediments: Evidence from a contemporary tidewater glacier, Spitsbergen, *Quat. Int.*, *86*, 71–79.
- Carr, S. J., and J. Rose (2003), Till fabric patterns and significance: Particle response to subglacial stress, *Quat. Sci. Rev.*, *22*, 1415–1426.
- Cladouhos, T. T. (1999), A kinematic model for deformation within brittle shear zones, *J. Struct. Geol.*, *21*, 437–448.
- Clark, P. U., and A. K. Hansel (1989), Clast ploughing, lodgement, and glacier sliding over a soft glacier bed, *Boreas*, *18*, 201–207.
- Clarke, G. K. C. (2005), Subglacial processes, *Ann. Rev. Earth Planet. Sci.*, *33*, 247–276.
- Day, R., M. Fuller, and V. A. Schmidt (1977), Hysteresis properties of titanomagnetites: Grain-size and compositional dependence, *Phys. Earth Planet. Inter.*, *13*, 260–267.
- Dowdeswell, J. A., and M. J. Sharp (1986), Characterization of pebble fabrics in modern terrestrial glaciogenic sediments, *Sedimentology*, *33*, 699–710.
- Dowdeswell, J. A., and M. J. Siegert (1999), Ice-sheet numerical modeling and marine geophysical measurements of glacier-derived sedimentation on the Eurasian Arctic continental margins, *Geol. Soc. Am. Bull.*, *111*, 1080–1097.
- Dunlop, D. J. (2002), Theory and application of the Day plot ( $M_r/M_s$  versus  $H_c/H_s$ ) 1. Theoretical curves and tests using titanomagnetite data, *J. Geophys. Res.*, *107*(B3), 2056, doi:10.1029/2001JB000486.
- Dunlop, D. J. and Ö. Özdemir (1997), *Rock Magnetism: Fundamentals and Frontiers*, 573 pp., Cambridge Univ. Press, New York.
- Easterbrook, D. J. (1988), Paleomagnetism of Quaternary deposits, *Spec. Pap. Geol. Soc. Am.*, *227*, 111–122.
- Engelhardt, H., and B. Kamb (1997), Basal hydraulic system of a West Antarctic Ice Stream: Constraints from borehole observations, *J. Glaciol.*, *43*, 207–230.
- Engelhardt, H., and B. Kamb (1998), Basal sliding of Ice Stream B, west Antarctica, *J. Glaciol.*, *44*, 223–230.
- Eyles, N., T. E. Day, and A. Gavican (1987), Depositional controls on the magnetic characteristics of lodgement tills and other glacial diamict facies, *Can. J. Earth Sci.*, *24*, 2436–2458.
- Fowler, A. C. (2000), An instability mechanism for drumlin formation, Deformation of glacial materials, *Geol. Soc. Spec. Pub.*, *176*, 307–319.
- Fuller, M. D. (1964), A magnetic fabric in till, *Geol. Mag.*, *99*, 233–237.
- Gravenor, C. P., M. Stupavsky, and D. T. Symonds (1973), Paleomagnetism and its relationship to till deposition, *Can. J. Earth Sci.*, *10*, 1068–1078.
- Grommé, G. S., T. L. Wright, and D. L. Peck (1969), Magnetic properties and oxidation of iron-titanium oxide minerals in Alae and Makaopuhi lava lakes, Hawaii, *J. Geophys. Res.*, *74*, 5277–5294.
- Ham, N. H., and D. M. Mickelson (1994), Basal till fabric and deposition at Burroughs Glacier, Glacier Bay, Alaska, *Geol. Soc. Am. Bull.*, *106*, 1552–1559.
- Hart, J. K. (1994), Till fabric associated with deformable beds, *Earth Surf. Processes Landforms*, *19*, 15–32.
- Hart, J. K. (1997), The relationship between drumlins and other forms of subglacial glaciotectionic deformation, *Quat. Sci. Rev.*, *16*, 93–107.
- Hayman, N. W., B. A. Housen, T. T. Cladouhos, and K. Livi (2004), Magnetic and clast fabrics as measurements of grain-scale processes within the Death Valley shallow crustal detachment faults, *J. Geophys. Res.*, *109*, B05409, doi:10.1029/2003JB002902.
- Head, K. H. (1989), *Soil Technician's Handbook*, 83 pp., John Wiley, New York.
- Hicock, S. R., and A. Dreimanis (1992), Deformation till in the Great Lakes regions: Implications for rapid flow along the south-central margin of the Laurentide Ice Sheet, *Can. J. Earth Sci.*, *29*, 1565–1579.
- Hicock, S. R., J. R. Goff, O. B. Lian, and E. C. Little (1996), On the interpretation of subglacial till fabric, *J. Sediment. Res.*, *66*, 928–934.
- Hindmarsh, R. C. A. (1988), Drumlinization and drumlin-forming instabilities: Viscous till mechanisms, *J. Glaciol.*, *44*, 293–314.
- Hooke, R. L., and A. Elverhøi (1996), Sediment flux from a fjord during glacial periods, Isfjorden, Spitsbergen, *Global Planet. Change*, *12*, 237–249.
- Hooyer, T. S., and N. R. Iverson (2000a), Clast-fabric development in a shearing granular material: Implications for subglacial till and fault gouge, *Geol. Soc. Am. Bull.*, *112*, 683–692.
- Hooyer, T. S., and N. R. Iverson (2000b), Diffusive mixing between shearing granular layers: Constraints on bed deformation from till contacts, *J. Glaciol.*, *46*, 641–651.
- Hrouda, F., and J. Ježek (1999), Theoretical models for the relationship between magnetic anisotropy and strain: Effect of triaxial magnetic grains, *Tectonophysics*, *301*, 183–190.
- Iverson, N. R., R. Baker, and T. S. Hooyer (1997), A ring-shear device for the study of till deformation: Tests on a clay-rich and a clay-poor till, *Quat. Sci. Rev.*, *16*, 1057–1066.
- Iverson, N. R., T. S. Hooyer, and R. Baker (1998), Ring-shear studies of till deformation: Coulomb-plastic behavior and distributed strain in glacier beds, *J. Glaciol.*, *44*, 634–642.
- Jeffery, G. B. (1922), The motion of ellipsoidal particles immersed in a viscous fluid, *Proc. R. Soc. London Ser. A*, *102*, 169–179.
- Jelinek, V. (1978), Statistical processing of anisotropy of magnetic susceptibility measured on groups of specimens, *Stud. Geophys. Geod.*, *22*, 50–62.
- Jelinek, V. (1981), Characterization of Magnetic fabric of rocks, *Tectonophysics*, *79*, 563–567.
- Jenson, J. W., P. U. Clark, D. R. MacAyeal, C. Ho, and J. C. Vela (1995), Numerical modeling of advective transport of saturated deforming sediment beneath the Lake Michigan Lobe, Laurentide Ice Sheet, *Geomorphology*, *14*, 157–166.
- Jenson, J. W., D. R. MacAyeal, P. U. Clark, C. L. Ho, and J. C. Vela (1996), Numerical modeling of subglacial sediment deformation: Implications for the behavior of the Lake Michigan Lobe, Laurentide Ice Sheet, *J. Geophys. Res.*, *101*(B4), 8717–8728.
- Johnson, M. D. (1983), The origin and microfabric of Lake Superior Lobe red clay, *J. Sediment. Petrol.*, *53*, 859–873.
- Johnson, W. H., and A. K. Hansel (1999), Wisconsinan Episode glacial landscape of central Illinois: A product of subglacial deformation processes?, *Spec. Pap. Geol. Soc. Am.*, *337*, 121–136.
- Jørgensen, F., and J. A. Piotrowski (2003), Signature of the Baltic Ice Stream on Funen Island, Denmark during the Weichselian glaciation, *Boreas*, *32*, 242–255.
- Kjær, K., and J. Krüger (1998), Does clast size influence fabric strength?, *J. Sediment. Res.*, *68*, 746–749.
- Lagroix, F., and S. K. Banerjee (2002), Paleowind directions from the magnetic fabric of loess profiles in central Alaska, *Earth Planet. Sci. Lett.*, *195*(1–2), 99–112.
- Lagroix, F., and S. K. Banerjee (2004), The regional and temporal significance of primary aeolian magnetic fabrics preserved in Alaskan loess, *Earth Planet. Sci. Lett.*, *225*(3–4), 369–385.
- Larsen, N. K., J. A. Piotrowski, and C. Kronborg (2004), A multiproxy study of a basal till: A time-transgressive accretion and deformation hypothesis, *J. Quat. Sci.*, *19*, 9–21.
- Larsen, N. K., J. A. Piotrowski, and F. Christiansen (2006), Microstructures and microshears as proxy for strain in subglacial diamicts: Implications for basal till formation, *Geology*, *34*(10), 889–892.
- Lawson, D. E. (1979), A comparison of pebble orientations in ice and deposits of the Matanuska Glacier, Alaska, *J. Glaciol.*, *87*, 629–645.
- Maltman, A. (1987), Shear zones in argillaceous sediments—an experimental study, *Geol. Soc. Spec. Publ.*, *29*, 77–87.
- Mark, D. M. (1973), Analysis of axial orientation data, including till fabrics, *Geol. Soc. Am. Bull.*, *84*, 1369–1374.
- Menzies, J. (2000), Micromorphological analyses of microfabrics and microstructures indicative of deformation processes in glacial sediments, *Geol. Soc. Spec. Publ.*, *176*, 245–258.
- Ó Cofaigh, C., R. D. Larter, J. A. Dowdeswell, C.-D. Hillenbrand, C. J. Pudsey, J. Evans, and P. Morris (2005), Flow of the West Antarctic Ice Sheet on the continental margin of the Bellingshausen Sea at the Last Glacial Maximum, *J. Geophys. Res.*, *110*, B11103, doi:10.1029/2005JB003619.
- Owens, W. H. (1974), Mathematical model studies on factors affecting the magnetic anisotropy of deformed rocks, *Tectonophysics*, *24*, 115–131.
- Skempton, A. W. (1985), Residual strength of clays in landslides, folded strata, and the laboratory, *Geotechnique*, *35*, 3–18.
- Stupavsky, M., and C. P. Gravenor (1975), Magnetic fabric around boulders in till, *Geol. Soc. Am. Bull.*, *86*, 1534–1536.
- Stupavsky, M., D. T. A. Symonds, and C. P. Gravenor (1974a), Paleomagnetism and magnetic fabric of the Leaside and Sunnybrook tills near Toronto, Ontario, *Geol. Soc. Am. Bull.*, *85*, 1233–1236.
- Stupavsky, M., and C. P. Gravenor (1974b), Paleomagnetism of the Port Stanley till, Ontario, *Geol. Soc. Am. Bull.*, *85*, 141–144.
- Tarling, D. H., and F. Hrouda (1993), *The Magnetic Anisotropy of Rocks*, 217 pp., Chapman and Hall, London.
- Thomason, J. F. (2006), Laboratory studies of till deformation with implications for the motion and sediment transport of the Lake Michigan Lobe, Ph.D. thesis, Iowa State Univ., Ames.
- Thomason, J. F., and N. R. Iverson (2006), Microfabric and microshear evolution in deformed till, *Quat. Sci. Rev.*, *25*, 1027–1038.
- Tika, T. E., P. R. Vaughan, and L. J. Lemos (1996), Fast shearing of pre-existing shear zones in soil, *Geotechnique*, *46*, 197–233.
- Tulaczyk, S., W. B. Kamb, and H. F. Engelhardt (2000), Basal mechanics of Ice Stream B, West Antarctica 1. Till mechanics, *J. Geophys. Res.*, *105*(B1), 463–481.
- van der Meer, J. J. M., J. Menzies, and J. Rose (2003), Subglacial till: The deforming glacier bed, *Quat. Sci. Rev.*, *22*, 1659–1685.

van der Wateren, F. M., S. J. Kluiving, and L. R. Bartek (2000), Kinematic indicators of subglacial shearing, *Geol. Soc. Spec. Publ.*, 176, 259–278.

---

T. S. Hooyer, Wisconsin Geological and Natural History Survey, University of Wisconsin, 3817 Mineral Point Road, Madison, WI 53705, USA. (tshooyer@wisc.edu)

N. R. Iverson, Department of Geological and Atmospheric Sciences, Iowa State University, Ames, IA 50011, USA. (niverson@iastate.edu)

F. Lagroix, Equipe de Paléomagnétisme, Institut de Physique du Globe de Paris, Université Paris Diderot, CNRS, 4 place Jussieu, Tour 14–15, 2ième étage, bureau 220, F-75252 Paris Cedex 05, France. (lagroix@ipgp.jussieu.fr)

J. F. Thomason, Illinois State Geological Survey, 615 East Peabody Drive, Champaign, IL 61820, USA. (thomason@isgs.uiuc.edu)